WARSAW UNIVERSITY OF TECHNOLOGY Index 351733
FACULTY OF CIVIL ENGINEERING
COMMITTEE FOR CIVIL AND WATER ENGINEERING
POLISH ACADEMY OF SCIENCES ISSN 1230-2945

DOI: 10.24425/ace.2023.146103

ARCHIVES OF CIVIL ENGINEERING

Vol. LXIX ISSUE 3 2023

pp. 645 –663

Research paper

Analysis of the seismic performances of structures reinforced by self-centering buckling-restrained braces

Yongxu Jin[1], Man Xu[2], Jie Jia[3]

Abstract: The self-centering buckling-restrained brace (SC-BRB) may achieve self-restoration for structures and, to a certain degree, diminish the substantial seismic residual deformation following rare earthquakes when compared to the usage of the conventional buckling-restrained brace (BRB). It may be possible to reduce the abrupt change in stiffness at the location of the strengthened stories and make the outrigger better at dissipating energy by improving the design of the energy-dissipation outrigger. This study compares the seismic performances of two types of energy-dissipation outriggers with BRB and SC-BRB web member designs during rare earthquakes so that the changes can be measured. The results show that using the SC-BRB web member design reduces the maximum inter-story drift ratio by an average of 7.68% and increases the average plastic-energy dissipation of the outrigger truss by 8.75%. The evaluation results show that the SC-BRB outrigger truss structure has better structural regularity and energy-dissipation performance. It has the ability to efficiently regulate the structural seismic response and lessen primary-structure damage.

Keywords: super-high raise building, self-centering buckling-restrained brace, outrigger truss, energy dissipation

[1]ME., College of Civil Engineering, Northeast Forestry University, Harbin 150040, China, e-mail: anzaichika@126.com, ORCID: 0000-0001-6268-0353

[2]Prof., PhD., College of Civil Engineering, Northeast Forestry University, Harbin 150040, China, e-mail: xuman306@126.com, ORCID: 0000-0001-6571-5101

[3]Prof., PhD., College of Civil Engineering, Northeast Forestry University, Harbin 150040, China, e-mail: jiajie@nefu.edu.cn, ORCID: 0000-0002-6906-2977

1. Introduction

With the increasing complexity of the design of super-high raise buildings in cities, improving the seismic resilience of such structures has become an important direction in current seismic research in engineering [1,2]. Recent studies have shown that when the BRB web member design is employed for the outrigger truss, the benefits of the outrigger truss as a way to reduce the effects of earthquakes and dissipate energy are enormous [3,4]. The original energy dissipation through the plastic hinge of the beam is changed to concentrated energy dissipation only in the BRB web members, better protecting the main structure. In tension and compression, BRB can reach full cross-sectional yielding without damaging the support members globally or locally [3]. The outrigger coordinates the stiffness distribution between the frame and the core tube to reduce the top displacement and the bottom bending moment in the frame-core tube structure [5]. At the same time, the device avoids the problem that the conventional steel truss design must increase the section size of steel web members to reach the required design strength. This causes a sharp increase in the overall stiffness of the outrigger and weakens its mechanical performance [6].

However, in order to allow for the dissipation of structural mechanical energy into internal energy [7], BRB web members rely primarily on plastic deformation of their core materials, which causes unrecoverable seismic residual deformation of the web members after earthquakes, jeopardizing the stability of the frame-core tube structure [8]. The main constraint on further improving the energy-dissipation capability of BRB web members is the large seismic residual deformation that remains after rare earthquakes [9]. By using a SC-BRB, which has a strong foreground, it is possible to effectively weaken the seismic residual deformation of BRB web members after an earthquake. When SC-BRB is used, web members can achieve structural self-restoration, and damage from plastic deformation to the structure can be kept to a minimum [10–13].

The SC-BRB, based on prestressing technology, takes into account both engineering issues and the realization approach for self-restoration. Currently, it continues to be the primary design for optimization.

The first SC-BRB with considerable axial strain was suggested by Chnstopoulos et al. [14]. Pre-stressed aramid fibers are primarily responsible for the restoring force, while metal friction is responsible for dissipating energy. The SC-BRB has a flag-shaped hysteresis curve and excellent self-restoration and energy-dissipation abilities. This is better than conventional BRB, which had unrecoverable seismic residual deformation after earthquakes. Using ANSYS, Tan et al. [15] examined how the steel-framed structure with SC-BRB and the steel-framed structure with BRB performed in earthquakes. The results showed that the SC-BRB obviously reduced the structure's seismic residual deformation.

As the structural building off-gauge design is becoming increasingly prevalent, the BRB web member of the outrigger truss is no longer sufficient to meet the seismic residual deformation limit demands of super-tall building structures during rare earthquakes. The SC-BRB is better for use in areas with high-intensity earthquakes because its self-restoration system is more flexible and can be controlled, changed, and adjusted more accurately to meet engineering requirements [16].

Several researchers have conducted numerical simulations and studies on the design scheme of the SC-BRB project, including Chou et al. [17], Tremblay [18], Xie [19], and Liu [20, 21] These studies have shown that SC-BRB plays an important role in controlling the residual deformation of the structure and improving its support capacity and performance. Liu [20, 21] proposed a design scheme for the nonlinear displacement ratio based on the results of a large number of numerical simulations of the single-degree-of-freedom system, which can be applied to the displacement-based design of the SC-BRB framework.

One previous study from Zhang [16] proposed to convert the steel web members of outrigger trusses to BRB web members in order to improve their ability to dissipate energy. The results show that the energy dissipation of BRB web members has greatly improved. Few studies, however, have compared the seismic performances of SC-BRB and BRB web members in outrigger trusses. In practice, SC-BRB has been widely applied in the seismic design of various high-rise buildings. Studies above have shown that structures designed with SC-BRB can significantly reduce residual deformation after earthquakes, enhance their seismic resistance and ductility, and reduce the cost and difficulty of repair compared to traditional BRB. Therefore, the SC-BRB technology has broad application prospects and can provide more reliable and economical solutions for the seismic design of high-rise buildings. Based on Liu's experimental design and quasistatic test for the SC-BRB [20, 21], this work suggests changing the BRB web members of outrigger trusses to the SC-BRB web members. ABAQUS was used to model BRB and SC-BRB web members, and the three indicators of how well a building handles earthquakes – the inter-story drift ratio, the base bending moment, and the base shear – were looked at with a focus on six rare earthquakes. To further assess the damage control of the different energy-dissipation outrigger trusses on the system during rare earthquakes, the plastic-energy dissipation contribution of the important structural components was thoroughly computed. This paper is intended to provide a theoretical framework for the use of innovative SC-BRB energy dissipation outrigger trusses in engineering applications.

2. Overview of the construction project

The background engineering was a real frame-core-tube structure, and the corresponding finite-element model was created to ensure the study's accuracy. The outer-frame columns are steel-reinforced-concrete columns, the outer-frame beams are steel beams, and the steel beams connect the floor between the outer frame and the core tube. The site classification for construction is Class II, the seismic design grouping is Group I, the seismic intensity is 8 degrees, and the design basis earthquake ground motion is 0.30 g [22]. The building has a total of 55 floors on the ground, and its total height is 238.5 meters. The height of each floor with outrigger trusses is 5.5 meters. The structural plan of the 33rd floor with outrigger trusses is shown in Fig. 1a and the ABAQUS 3D model is shown in Fig. 2b). The outrigger trusses are evenly and symmetrically arranged along the X and Y axes and are installed on the 17th, 33rd, and 55th floors, and the web members are constructed of conventional steel braces.

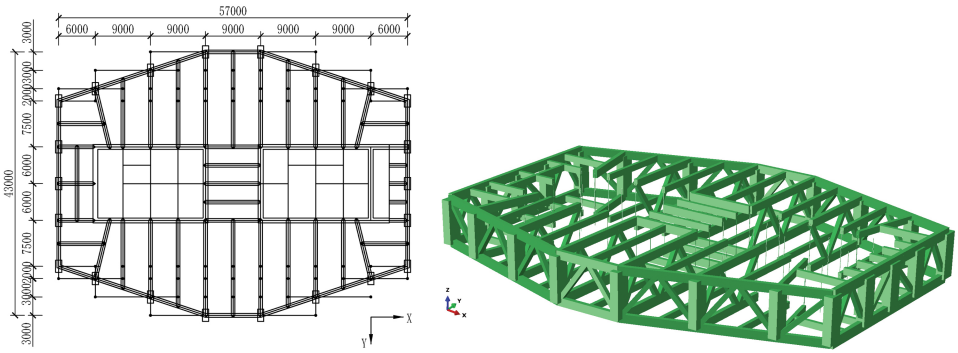

(a) (b)

Fig. 1. The 33rd floor with outrigger trusses (units in Figure 1 (a) are in millimeters)

3. Establishment of finite-element model

3.1. Establishment of structural finite-element model

Figure 2 shows the ABAQUS 3D model of the overall structure, which marks the outrigger location of the frame-core-tube structure. The YJK building program (YJK) [23] was used to establish the finite-element model of the frame-core-tube structure and convert it to the ABAQUS model. The model contains 325,052 structural units and 22,048 nodes. The "B31" beam elements were used for the beams and columns; the "S4R" shell elements were used for the walls and floors; and the "T3D2" truss elements were used for the outrigger trusses. The beams and slabs were filled with C40-level concrete, whereas the columns and walls were filled with C45-level concrete [24]. The structural steels on outrigger trusses were Q345 steel [25], and the elastic–plastic dou-ble-line model as well as the

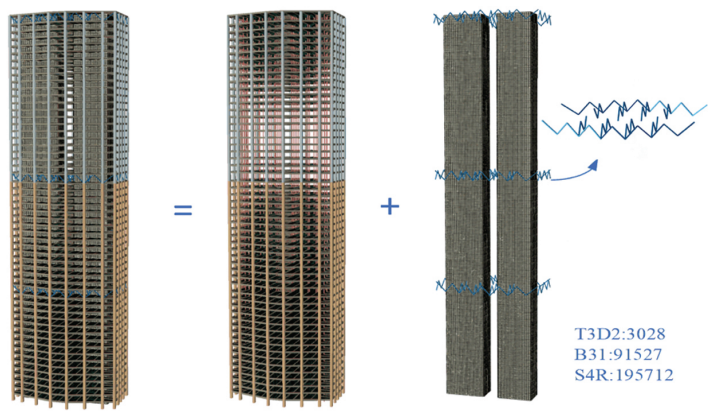

Fig. 2. FEM of the frame-core-tube structure

concrete damage plasticity model were used. Under load, the deformation of the structure accounts for the majority of the overall deformation. In order to facilitate convergence and accelerate model computation, an ideal elastic-plastic constitutive relationship is adopted for the steel material in this article. The elastic modulus of the steel material is 200 GPa, the Poisson's ratio is 0.3, and the standard yield strength of Q345 steel is 345 MPa. The average yield strength of the steel material is taken as 1.1 times the standard value, which is 379.5 MPa. The bottom of the first floor was subjected to displacement restrictions in order to satisfy the foundation that there is no displacement in the horizontal direction. The ABAQUS model converted by YJK was used to perform the seismic-response calculation and energy-dissipation analysis to guarantee the correctness of the finite-element model.

The concrete in this project was modeled using the "concrete damaged plasticity" material model, while all longitudinal rebars, stirrups, steels, BRBs and SC-BRBs were modeled using the bilinear material model [26].

3.2. Establishment of the finite-element model for BRB web members

This section established the finite-element model for BRB web members based on the quasi-static test and finite element verification work of Yang et al.'s BRB [3, 27].

A BRB is composed of four elements: an inner steel core, which is the yielding element; a bond-preventing layer around the inner core; an outer steel casing (round or square); and grout infill, which provides stability to the inner core. Therefore, the steel inner core is fully braced within the steel outer casing and the grout, such that it can yield in tension and compression without buckling [28, 29].

Using the sweep, the steel outer casing and the energy-dissipation inner core both have a mesh size of 50 mm. The C3D8R elements were used throughout while establishing the finite-element model of BRB in ABAQUS. The inner core of the BRB that was designed as a cross section was made of BLY225 [30] low-yield-point steel with a yield stiffness of 225 MPa that is used for seismic resistance. Furthermore, C30-level concrete [24] was utilized as the grout. The steel outer casing was made of Q345 steel with the elastic–plastic double-line model. The interaction between the steel outer casing and the inner core was modeled by contact. Simulating the contact behavior between different components by defining the method of "surface-to-surface contact". In this method, the normal behavior is defined as "hard" contact [30], while the tangential behavior is defined using a "penalty" function [31]. This approach can simulate the behavior of different types of contacts and provide relatively accurate simulation results. Tie constraints were used to simulate the connection between the web member and the frame, simplifying the analysis and accelerating the computation. The beam unit was used as the basis for setting up the material's constitutive model. The web-member-cross-section size of the BRB is shown in Fig. 3. Figure 4 shows the loading protocol in ABAQUS. Adopting displacement-based load control method, the load-displacement-value refer to Liu et al. [20, 21] settings are, in order, 1/1000, 1/500, 1/100, 1/80, 1/50, 1/30, and 1/20 of the length of the web member. The BRB stress contour is shown in Fig. 5. The BRB hysteresis curve is shown in Fig. 6.

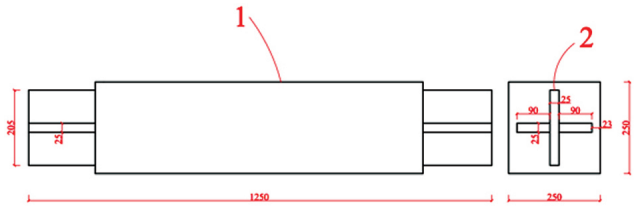

Fig. 3. The BRB web-member-cross-section size; 1 – Steel outer casing, 2 – inner core

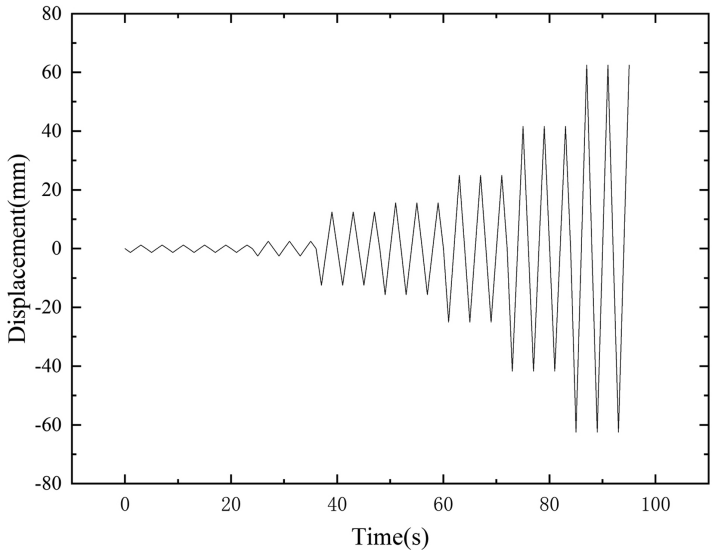

Fig. 4. Loading protocol

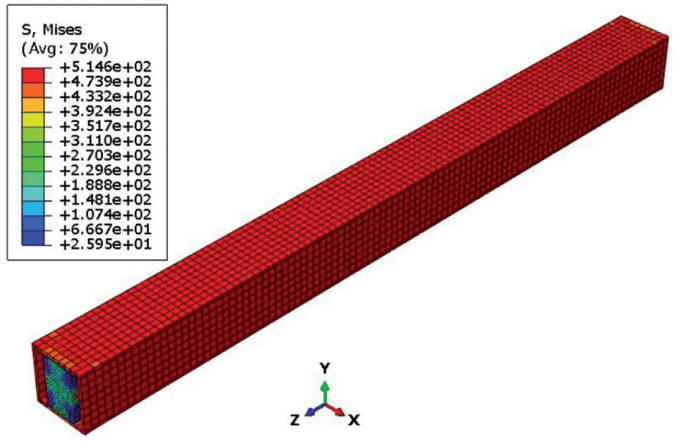

Fig. 5. The BRB stress contour

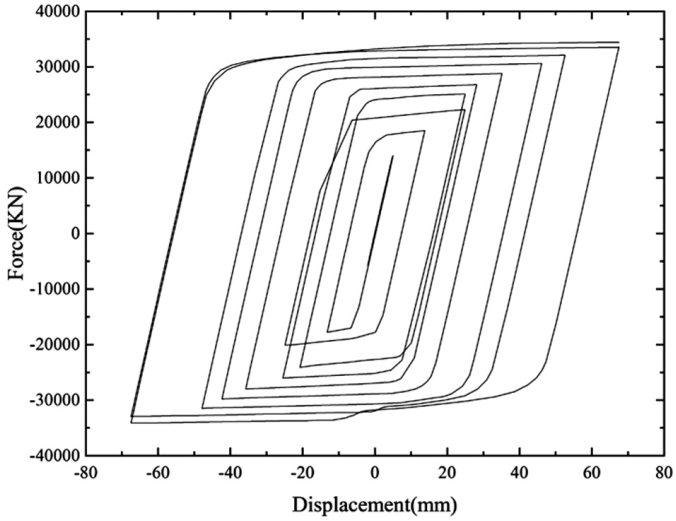

Fig. 6. The BRB hysteresis curve

3.3. Establishment of the finite-element model for SC-BRB web member

Based on the experimental design and quasi-static test of Liu et al.'s SC-BRB [20, 21], this section established the finite-element model for SC-BRB web members. The SC-BRB web-member-design plan is shown in Fig. 7.

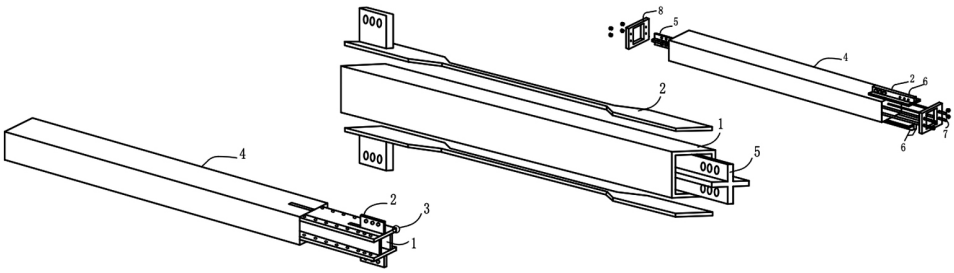

Fig. 7. The SC-BRB web-member-design plan; 1 – steel inner casing, 2 – inner core, 3 – intermediate-constraint force-transmission element, 4 – steel outer casing, 5 – internal adapting piece, 6 – outer adapting piece, 7 – prestressed tendons, 8 – end plates

Using the sweep, the steel outer casing and the energy-dissipation inner core both have the same mesh size as the BRB. The end plate has a mesh size of 20 mm, and the prestressed tendon has a mesh size of 120 mm.

The inner core of the SC-BRB is made of BLY225 low-yield-point steel, the tendons were simulated using the T3D2 truss elements, and the other components were manu-

factured using the C3D8R elements when the finite-element model of the SC-BRB web members was established in ABAQUS. C30-level concrete was utilized as the grout.

The prestressed tendon was connected by partially embedding the end plates; contact was used to model the interaction between the steel outer casing and the inner core; embedding was used to model the interaction between the prestressed tendon and the grout; contact was used to connect the energy-dissipation inner core and the grout. Tie constraints were used to simulate the connection between the web member and the frame, simplifying the analysis and accelerating the computation. The HRB335 [32] was used as the basis for setting up the material's constitutive model. Simulating the contact behavior between different components are the same as the BRB web member.

Table 1 shows the dimensions of the SC-BRB's main components. The same loading protocol as in the BRB was used. Figure 8 depicts the SC-BRB stress contour. Figure 9 depicts the SC-BRB hysteresis curve. Figure 10 compares the hysteresis curves of the BRB and the SC-BRB.

Table 1. Dimensions of the SC-BRB's Main Components

Components	Cross-section size	Number
Steel inner casing	$180 \times 180 \times 6 \times 6$ mm	1
Steel outer casing	$150 \times 150 \times 6 \times 6$ mm	1
Inner core	24×6 mm	2
Prestressed tendon	75	4
End plate	$180 \times 180 \times 30$ mm (Hole-cutting Size)	2

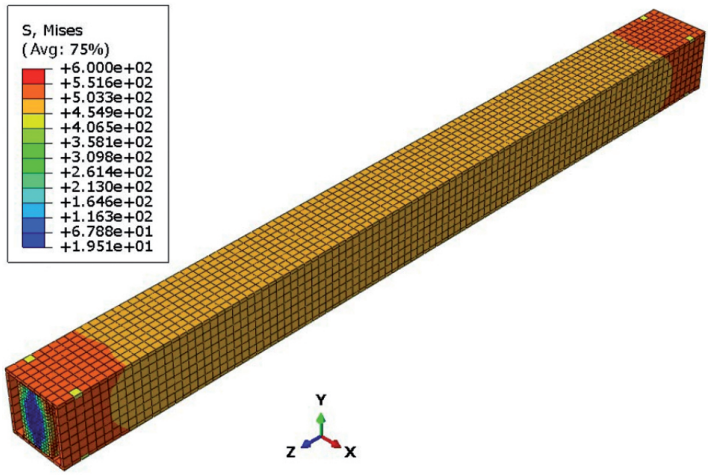

Fig. 8. The SC-BRB stress contour

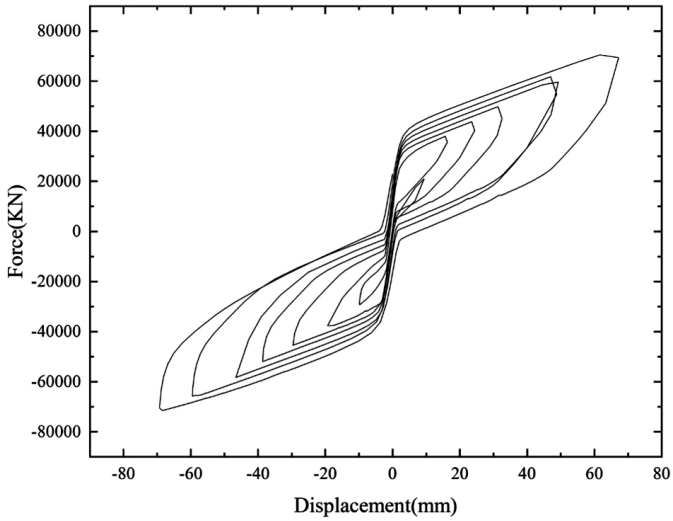

Fig. 9. The SC-BRB hysteresis curve

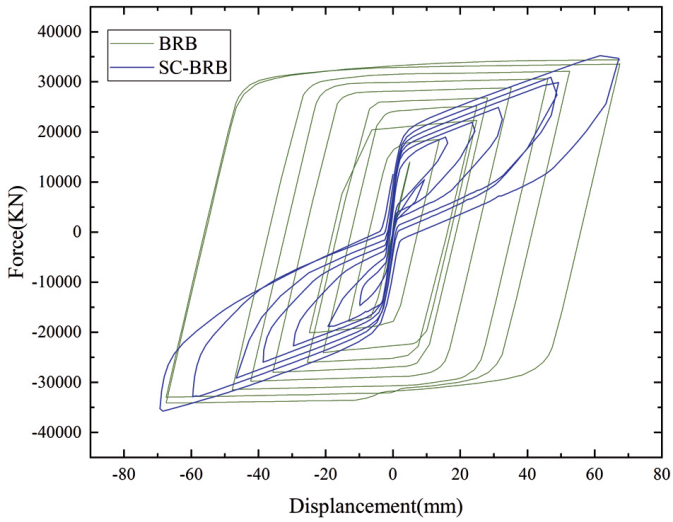

Fig. 10. Comparison of the hysteresis curves of the BRB and SC-BRB

4. Seismic performances of structures

4.1. Selection and input of seismic motions

The difference between the base-shear and response-spectrum methods, when compared, shows that a single seismic-motion error does not surpass 35%. The standard deviation is not 20%. Five natural seismic motions were chosen. The YJK simulated a single

artificial seismic motion with a peak ground acceleration (PGA) of 400 cm/s^2, which is consistent with the seismic motion of a magnitude 8 earthquake. Figure 11 compares the seismic-motion spectrum (after amplitude modulation) to the standard response spectrum.

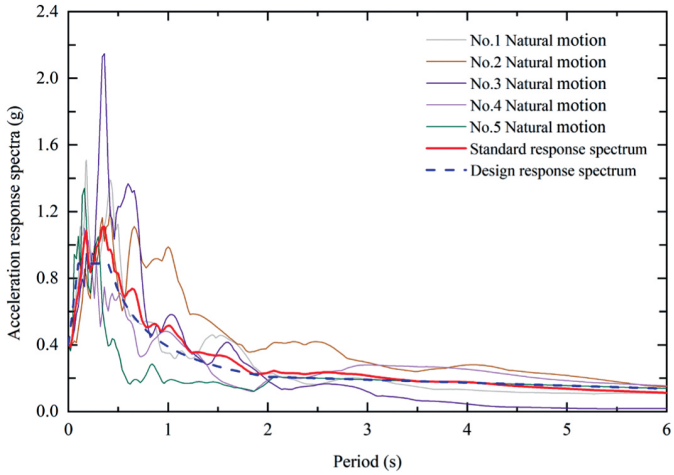

Fig. 11. Response spectrum

4.2. The inter-story-drift ratio

The inter-story-drift ratio of the structure, which is considered the primary reference factor for determining the stiffness of the structure in the horizontal direction, has a strong correlation with the structural damages due to the multi-physical coupling phenomena of different structural elements [33]. Furthermore, the size of the inter-story-drift ratio has a direct influence on the cross-sectional area and stiffness of the web members of the out-rigger trusses. As shown in Fig. 12 and Table 2, monitoring the maximum value of the Y-directional inter-story drift ratio is an important task that is required for both models based on the input seismic motions.

The results show that the frame-core-tube structure with SC-BRB outrigger trusses has a slightly smaller inter-story drift ratio than the structure with BRB outrigger trusses on the middle and upper floors. The inter-story-drift ratio drops most noticeably when the No. 5 natural motion happens. The maximum reduction amplitude reaches 10.80%, and the average reduction amplitude when 6 seismic motions happen is about 7.68%. All the maximum inter-story-drift ratios are in the positive direction.

Since the original structural outrigger trusses were constructed as steel-braced web members, the replacement of all the steel-braced web members in the original structure using the BRB web members are comparable to a comprehensive optimization of the original system. Additionally, the steel-reinforced-concrete columns strengthen the lateral stiffness of the original structure. When the web-member design is once again changed to

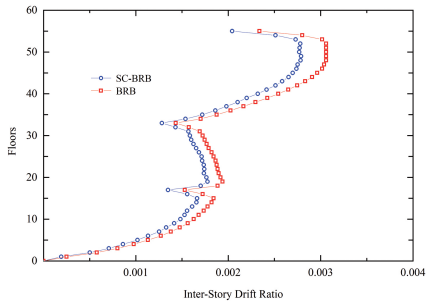

(a) No. 1 Natural motion +Y

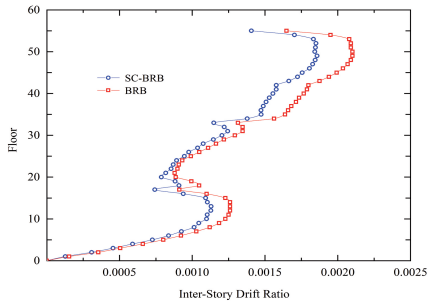

(b) No. 1 Natural motion –Y

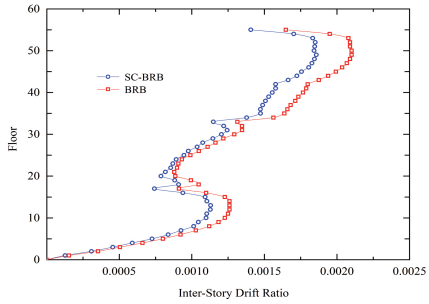

(c) No. 2 Natural motion +Y

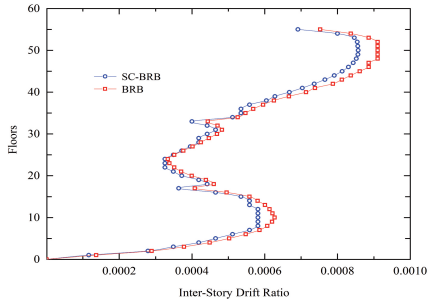

(d) No. 2 Natural motion –Y

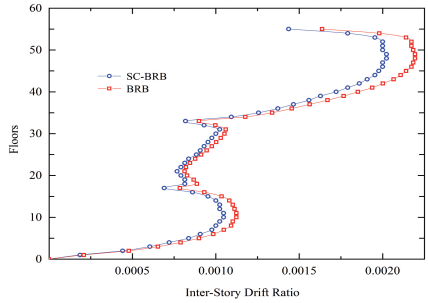

(e) No. 3 Natural motion +Y

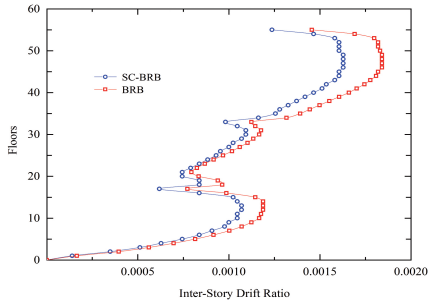

(f) No. 3 Natural motion –Y

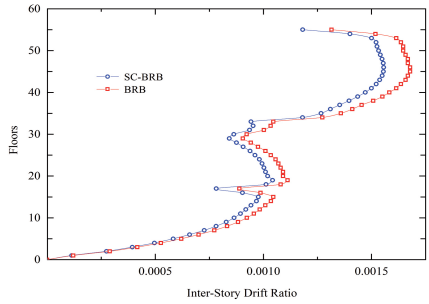

(g) No. 4 Natural motion +Y

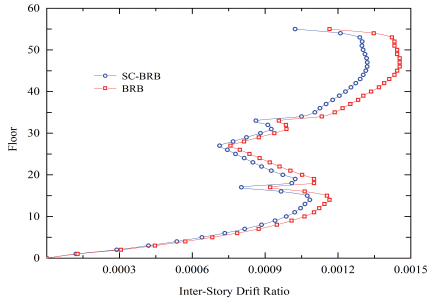

(h) No. 4 Natural motion –Y

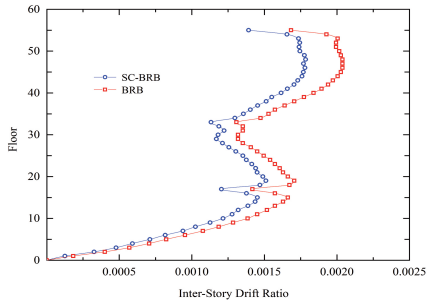

(i) No. 1 Natural motion +Y

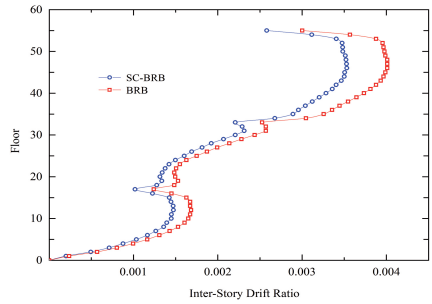

(j) No. 1 Natural motion –Y

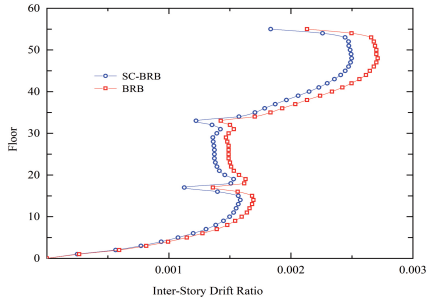

(k) Artificial seismic motion +Y

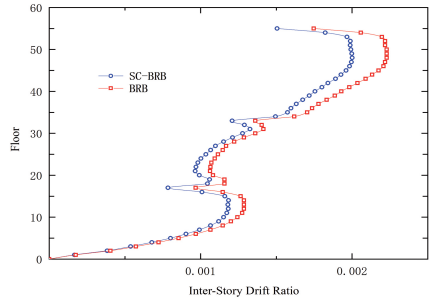

(l) Artificial seismic motion –Y

Fig. 12. The inter-story-drift ratio of the structures; the maximum positive displacement in the inter-story-drift ratio in the Y direction is represented by +Y, while the maximum negative displacement in the Y direction is represented by –Y

Table 2. Comparison between BRB and SC-BRB effects in the inter-story-drift ratio under rare earthquakes

Seismic motion	Θ_{max}		
	SC-BRB	BRB	Reduction (%)
No. 1 natural motion	0.002788186	0.003038286	8.97
No. 2 natural motion	0.000856884	0.00090684	5.83
No. 3 natural motion	0.002023256	0.002164682	6.99
No. 4 natural motion	0.001556535	0.001664714	6.95
No. 5 natural motion	0.00178414	0.001976827	10.80
Artificial seismic motion	0.002497229	0.002660797	6.55
Average value			7.68

a SC-BRB design, it is normal and expected for the inter-story-drift ratio to decrease by a small amount.

Both BRB and SC-BRB outrigger trusses may effectively minimize the structure's inter-story-drift ratio since they both have strong energy-dissipation capabilities. But because of the significant post-earthquake seismic residual deformation, which in turn jeopardizes the integrity of the outrigger trusses, the energy-dissipation performance of BRB outrigger trusses cannot be further enhanced. Additionally, the control of the in-ter-story-drift ratio at the position where the outrigger truss is placed is more significantly affected by the SC-BRB outrigger truss. Consequently, the SC-BRB outrigger truss can effectively handle the movement of a super-tall structure during rare earthquakes.

4.3. Base-bending moment and base shear

It is dangerous to take the frame-core-tube structure's horizontal displacement as the sole indicator of instability and to neglect the complexity between the structural internal elements and the connections between the state variables. Based on the maximum values of the base-bending moment and base shear during earthquakes, it is important to assess the damage to the structure caused by the different designs of the web members. Table 3 shows the maximum values of the structure based on X- and Y-directional base-bending moments. Table 4 shows the maximum values of the structure based on X- and Y-directional base shear.

Table 3. Comparison of the base-bending moments

Seismic motion	M_{max} (KN·m)					
	X-directional			Y-directional		
	SC-BRB	BRB	Increase (%)	SC-BRB	BRB	Increase (%)
No. 1 natural motion	6300	5930	6.24	12700	11950	6.28
No. 2 natural motion	2660	2510	5.98	11000	10340	6.38
No. 3 natural motion	4900	4580	6.99	14800	14040	5.41
No. 4 natural motion	4600	4280	7.48	9750	9230	5.63
No. 5 natural motion	6540	5920	10.47	15000	13800	8.70
Artificial seismic motion	3170	2950	7.46	11640	10720	8.58
Average value			7.43			6.83

Compared to BRB outrigger trusses, SC-BRB outrigger trusses have a much stronger influence on the base bending moment and base shear of the structure. But the increase in the structure's Y-direction base-bending moment and X-direction base shear is minimal because of the structure's weaker stiffness in the Y direction. The X-directional base-bending moment and the Y-directional base-bending moment rise to their maxi-mum values when the No. 5 natural motion happens. When 6 seismic motions happen, the X-directional maximum increase reaches 10.47%, and the average value is about 7.43%; the Y-directional maximum increase reaches 8.70%, and the average value is about 6.83%. Similarly, the

Table 4. Comparison of the base shear

Seismic motion	F_{max} (KN)					
	X-directional			Y-directional		
	SC-BRB	BRB	Increase (%)	SC-BRB	BRB	Increase (%)
No. 1 natural motion	270000	255000	5.88	186000	167000	11.34
No. 2 natural motion	230000	218000	5.50	125000	110000	13.64
No. 3 natural motion	293000	278000	5.40	169000	151000	11.92
No. 4 natural motion	240000	228000	5.26	102000	91000	12.09
No. 5 natural motion	211400	198000	6.77	177000	145000	22.07
Artificial seismic motion	250000	235000	6.38	146000	129000	13.18
Average value			5.87			14.04

X-directional base shear and the Y-directional base shear rise to their maximum when the No. 5 natural motion happens. When 6 seismic motions happen, the X-directional maximum increase reaches 6.77%, and the average value is about 5.87%; the Y-directional maximum increase reaches 22.07%, and the average value is about 14.04%.

This shows that the SC-BRB web members can do a better job of increasing the base-bending moment and the base shear to protect the structure from rare earthquakes and make the system more stable.

5. Plastic-energy dissipation

Table 5 shows the structural plastic-energy dissipation as well as the proportion of structural plastic-energy dissipation in the total energy consumption during rare earthquakes.

Table 5 demonstrates that:

Compared to BRB outrigger trusses, SC-BRB outrigger trusses have significantly enhanced structural plastic-energy dissipation. When 6 seismic motions happen, the average incremental proportion of the structural plastic-energy dissipation in the total energy consumption reaches 0.94%. Among these, the incremental proportion of the structural plastic-energy dissipation in the total energy consumption reaches its maximum value when loading the No. 5 natural motion: 1.01% of the total energy consumption. The average increase in plastic-energy dissipation in the structure's outrigger trusses is 1.55×10^6 J when the design of the web members is changed from BRB web members to SC-BRB web members.

When the numerical value of structural plastic-energy dissipation is confirmed, the plastic-energy dissipation of the structure's important elements also has a critical influence on the seismic performance of the frame-core-tube structure. Table 6 shows the contribution of the important elements to the plastic-energy dissipation.

Table 5. Comparison of the plastic-energy-dissipation information of structures undergoing rare earthquakes

Seismic motion	FEM	Plastic-energy dissipation (J)	Proportion in the total energy consumption
No. 1 natural motion	BRB	1.60×10^7	23.11%
	SC-BRB	1.77×10^7	24.08%
	Increment	1.70×10^6	0.97%
No. 2 natural motion	BRB	0.97×10^7	13.35%
	SC-BRB	1.05×10^7	14.15%
	Increment	8.00×10^5	0.80%
No. 3 natural motion	BRB	1.81×10^7	21.04%
	SC-BRB	1.97×10^7	21.98%
	Increment	1.60×10^6	0.94%
No. 4 natural motion	BRB	1.26×10^7	26.73%
	SC-BRB	1.40×10^7	27.68%
	Increment	1.40×10^6	0.95%
No. 5 natural motion	BRB	1.50×10^7	23.49%
	SC-BRB	1.69×10^7	24.50%
	Increment	1.90×10^6	1.01%
Artificial seismic motion	BRB	1.46×10^7	21.22%
	SC-BRB	1.65×10^7	22.21%
	Increment	1.90×10^6	0.99%
Average value		1.55×10^6	0.94%

The plastic-energy dissipation of the structure's important elements during rare earthquakes was enumerated in order to better examine the influence of BRB and SC-BRB outrigger trusses. The carrying capacity of the structure will be somewhat reduced when the entire structure undergoes plastic deformation. However, the use of plastic-energy dissipation outrigger trusses can effectively control the plastic deformation that occurs during earthquakes, thereby reducing the degree of damage to the structure. At the same time, it can also increase the structure's residual carrying capacity, allowing it to maintain a certain degree of carrying capacity even after an earthquake occurs. When the energy-dissipation outrigger trusses are set up, the steel-reinforced-concrete columns essentially do not yield, so the discussion is mostly about the amount of plastic energy dissipation in the coupling beams, shear walls, and outrigger trusses.

Table 6 demonstrates that the coupling beam and the outrigger truss are the main structural energy-dissipation elements, followed by the shear wall. Comparing the plastic-energy dissipation of different structural elements, the average increase in the outrigger

Table 6. Comparison of the plastic-energy-dissipation proportion of structural parts undergoing rare earthquakes

Seismic motion	FEM	Outrigger truss	Coupling beam	Shear wall	Column
No. 1 natural motion	BRB	43.67%	32.43%	23.90%	0.00%
	SC-BRB	49.62%	25.14%	25.24%	0.00%
	Increment	7.95%	–7.29%	–1.34%	0.00%
No. 2 natural motion	BRB	39.16%	45.40%	15.44%	0.00%
	SC-BRB	47.23%	39.68%	13.09%	0.00%
	Increment	8.07%	–5.72%	–2.35%	0.00%
No. 3 natural motion	BRB	45.76%	33.18%	21.06%	0.00%
	SC-BRB	55.08%	26.34%	18.58%	0.00%
	Increment	9.32%	–6.84%	–2.48%	0.00%
No. 4 natural motion	BRB	55.90%	31.40%	12.65%	0.00%
	SC-BRB	64.73%	24.34%	10.93%	0.00%
	Increment	8.83%	–7.06%	–1.72%	0.00%
No. 5 natural motion	BRB	44.64%	36.85%	18.51%	0.00%
	SC-BRB	53.97%	29.52%	16.51%	0.00%
	Increment	9.33%	–7.33%	–2.00%	0.00%
Artificial seismic motion	BRB	42.63%	33.47%	23.90%	0.00%
	SC-BRB	51.60%	26.91%	21.49%	0.00%
	Increment	8.97%	–6.56%	–2.41%	0.00%
Average value		8.75%	–6.80%	–2.05%	0.00%

trusses is 8.75%, the average decrease in the coupling beams is 6.80%, and the average decrease in the shear walls is 2.05%. When the No. 5 natural motion is loaded, the outrigger trusses' incremental proportion goes up to its maximum value: 9.33%. It has the ability to efficiently regulate structural plastic-energy dissipation and increase structural stability. It may effectively reduce the damage caused by rare earthquakes to the coupling beams and the shear walls.

6. Conclusions and limitations

6.1. Conclusions

The excessive post-earthquake seismic residual deformation of BRB web members has been a drawback in the design of energy-dissipation outrigger trusses. The results of using the SC-BRB outrigger truss show that:

1. The frame-core-tube structure with SC-BRB outrigger trusses has a slightly smaller inter-story drift ratio than the structure with BRB outrigger trusses on the middle and upper floors. The maximum reduction amplitude reaches 10.80%, and the average reduction amplitude is about 7.68%.
2. In terms of the base-bending moment, the X-directional maximum increase reaches 10.47%, and the average value is about 7.43%; the Y-directional maximum increase reaches 8.70%, and the average value is about 6.83%. In terms of the base shear, the X-directional maximum increase reaches 6.77%, and the average value is about 5.87%; the Y-directional maximum increase reaches 22.07%, and the average value is about 14.04%.
3. The structural plastic-energy dissipation in the total energy consumption of the two buildings is basically the same. But comparing the plastic-energy dissipation of different structural elements, the average increase in the outrigger trusses is 8.75%, the average decrease in the coupling beams is 6.80%, and the average decrease in the shear walls is 2.05%.

The evaluation results show that the SC-BRB outrigger-truss structure has better structural regularity and energy-dissipation performance. It can better control how the structure reacts to rare earthquakes and reduce damage to the main structure.

6.2. Limitations

1. While the self-restoration system's features may effectively reduce seismic residual deformation, measuring seismic residual deformation with a multi-degree of freedom is extremely difficult. Therefore, this paper falls short in this regard.
2. It is more typical to use SC-BRB with prestressed tendons as the self-restoration system. In future papers, more creative and complicated self-restoration systems may be used to show a clearer difference in performances.
3. The current study does not provide any clear details on the simulation of the hysteretic behavior characterizing the vast majority of the structural elements adopted in the FE model. This may be addressed in future papers by implementing recent hysteresis models and adopting parameters that can be easily calibrated in ABAQUS.

References

[1] Z. Fang and P. Yan, "Influence of vertical ground motion on seismic responses of triple friction pendulum interlayer isolation structures", *Archives of Civil Engineering*, vol. 67, no. 3, pp. 581–597, 2021, doi: 10.24425/ace.2021.138072.

[2] F. Pachla and T. Tatara, "Nonlinear analysis of a hoist tower for seismic loads", *Archives of Civil Engineering*, vol. 68, no. 3, pp. 177–198, 2022, doi: 10.24425/ace.2022.141880.

[3] W. Zhen, Y.K. Qiu, Q.S. Yang, et al., "Energy dissipation performance of outrigger in tall buildings", *Engineering Mechanics*, vol. 38, no. 2, pp. 36–43, 2021, doi: 10.6052/j.issn.1000-4750.2020.10.ST08.

[4] H. Jiang and X.F. Zhao, "Performance analysis and experimental research of a super high-rise steel-reinforced concrete frame-corewall structure with outriggers in strengthened layers", *Journal of Building Structures*, vol. 50, no. 15, pp. 113–117+84, 2020, doi: 10.19701/j.jzjg.2020.15.021.

[5] J.A. Oviedo-Amezquita, N. Jaramillo-Santana, C.A. Blandon-Uribe, and A.M. Bernal-Zuluaga, "Development and validation of an acceptance criteria and damage index for buckling-restrained braces (BRB)", *Journal of Building Engineering*, vol. 43, art. no. 102534, 2021, doi: 10.1016/j.jobe.2021.102534.

[6] W. Zhen, "Energy dissipation performance of outrigger in super-tall buildings with outrigger systems", Beijing Jiaotong University, 2019.

[7] N. Vaiana, R. Capuano, and L. Rosati, "Evaluation of path-dependent work and internal energy change for hysteretic mechanical systems", *Mechanical Systems and Signal Processing*, vol. 186, art. no. 109862, 2023, doi: 10.1016/j.ymssp.2022.109862.

[8] Q. Xie, Z. Zhou, C. Li, and S. Meng, "Parametric analysis and direct displacement-based design method of self-centering energy-dissipative steel-braced frames", *International Journal of Structural Stability and Dynamics*, vol. 17, no. 8, art. no. 1750087, 2017, doi: 10.1142/S0219455417500870.

[9] W.N. Li, "Seismic performance analysis of self-centering buckling restrained brace", Taiyuan University of Technology, 2020.

[10] H. Zhang, P. Zeng, and C.L. Wang, "Performance study of self-centering buckling-restrained brace frame under bidirectional seismic action", *Industrial Construction*, vol. 49, no. 6, pp. 163–166+191, 2019, doi: 10.13731/j.issn.1000-4726.2017.05.028.

[11] Y. Chen, "Dissertation for Professional Master's Degree", Beijing University Of Civil Engineering And Architecture, 2021.

[12] H. Jiang and L.H. Xu, "Study on hysteretic performance of self-centering energy dissipation braces and seismic behaviors of braced frames", *Journal of Tianjin University (Science and Technology)*, vol. 54, no. 3, pp. 237–244, 2021.

[13] L.H. Xu and S.Q. Yao, "Experimental study and finite element simulation on hysteretic performance of self-centering energy dissipation brace", *Journal of Building Structures*, vol. 39, no. 11, pp. 158–165, 2018.

[14] C. Christopoulos, R. Tremblay, H.-J. Kim, et al., "Self-centering energy dissipative bracing system for the seismic resistance of structures: development and validation", *Journal of Structural Engineering*, vol. 134, no. 1, pp. 96–107, 2008, doi: 10.1061/(ASCE)0733-9445(2008)134:1(96).

[15] Y.Q. Tan, P.F. Wang, L.C. Huo, et al., "Analysis of the seismic performance of self – centering buckling – restrained brace steel frame", *Journal of Hebei University of Engineering (Natural Science Edition)*, vol. 31, no. 4, pp. 1–4, 2014.

[16] Y. Zhou, Y. Xiao, and A.Q. Gu, "Self-centering braced rocking frame systems and displacement-based seismic design method", *Journal of Building Structures*, vol. 40, no. 10, pp. 17–26, 2019, doi: 10.14006/j.jzjgxb.2019.0070.

[17] C.C. Chou, T. H. Wu, A.R.O. Beato, et al., "Seismic design and tests of a full-scale one-story one-bay steel frame with a dual-core self-centering brace", *Engineering Structures*, vol. 111, pp. 435–450, 2016, doi: 10.1016/j.engstruct.2015.12.007.

[18] R. Tremblay, M. Lacerte, and C. Christopoulos, "Seismic response of multistory buildings with self-centering energy dissipative steel braces", *Journal of Structural Engineering*, vol. 134, no. 1, pp. 108–120, 2008.

[19] Q. Xie, Z. Zhou, C. Li, et al., "Parametric analysis and direct displacement-based design method of self-centering energy-dissipative steel-braced frames", *International Journal of Structural Stability and Dynamics*, vol. 16, no. 7, art. no. 1750087, 2017, doi: 10.1142/S0219455417500870.

[20] L. Liu, B. Wu, W. Li, et al., "Cyclic tests of novel self-centering buckling-restrained brace", *Journal of Southeast University (Natural Science Edition)*, vol. 42, no. 3, pp. 536–541, 2012, doi: 10.3969/j.issn.1001-0505.2012.03.028.

[21] L. Liu, "Seismic bahavior and design of structure with self-centering buckling-restrained braces", Harbin Institute of Technology, 2013.

[22] National Standard of the People's Republic of China, *Code for Seismic Design of Buildings (GB 50011-2010)*. Beijing: China Architecture & Building Press, 2016.

[23] Beijing YJK Building Software Co., Ltd., *Structural calculation software: YJK-A's user manual and technical specifications*.

[24] China Architecture & Building Press, *Code for Design of Concrete Structures (GB 50010-2010)*. Beijing: China Architecture & Building Press, 2010.

[25] China Architecture & Building Press, *High Strength Low Alloy Structural Steels (GB/T 1591-2018)*. Beijing: China Architecture & Building Press, 2018.

[26] N. Staszak, T. Garbowski, and B. Ksit, "Application of the generalized nonlinear constitutive law in numerical analysis of hollow-core slabs", *Archives of Civil Engineering*, vol. 68, no. 2, pp. 125–145, 2022, doi: 10.24425/ace.2022.140633.

[27] Q.S. Yang, W. Zhen, L.L Xie, et al., "Experimental study on the seismic performance of energy dissipation outriggers", *Engineering Mechanics*, vol. 33, no. 10, pp. 76–85, 2016, doi: 10.6052/j.issn.1000-4750.2015.12.1013.

[28] H. Guerrero, A. Teran-Gilmore, E. Zamora, J.A. Escobar, and R. Gómez, "Hybrid simulation tests of a soft storey frame building upgraded with a Buckling-Restrained Brace (BRB)", *Experimental Techniques*, vol. 44, no. 5, pp. 553–572, 2020, doi: 10.1007/s40799-020-00378-5.

[29] Q. Chen, "Hysteretic properties of buckling-restrained braceds and seismic performance of buckling-restrained braced frames", Southeast University, 2016.

[30] K.G. Pu, F.M. Song, and D.H. Wen, "Development of low yield point steel heavy plate used for earthquake resistant", *Hot Working Technology*, vol. 40, no. 10, pp. 45–48, 2011, doi: 10.14158/j.cnki.1001-3814.2011.10.045.

[31] H. Ju, D. Lee, and D.U. Choi, "Finite element analysis of steel-concrete composite connection with prefabricated permanent steel form", *Journal of Asian Concrete Federation*, vol. 8, no. 1, pp. 1–15, 2022, doi: 10.18702/acf.2022.6.8.1.1.

[32] National Standard of the People's Republic of China, *Steel for the reinforcement of concrete (GB 1499-2018)*. China Planning Press, 2018.

[33] N. Vaiana and L. Rosati, "Classification and unified phenomenological modeling of complex uniaxial rate-independent hysteretic responses", *Mechanical Systems and Signal Processing*, vol. 182, art. no. 109539, 2023, doi: 10.1016/j.ymssp.2022.109539.

Received: 2022-12-26, Revised: 2023-04-06